SP1433-1438 operon of *Streptococcus pneumoniae* regulates metal homeostasis and cellular metabolism during zinc-stress

Lindsey R. Burcham[1], Rebecca A. Hill[2], Rachel C. Caulkins[1], Joseph P. Emerson[2], Bindu Nanduri[4], Jason W. Rosch[3], Nicholas C. Fitzkee[2], and Justin A. Thornton[1]*

[1]Department of Biological Sciences, Mississippi State University, Mississippi State, MS 39762, [2]Department of Chemistry, Mississippi State University, Mississippi State, MS 39762, [3]Department of Infectious Diseases, St. Jude Children's Research Hospital, Memphis, TN 38105, and [4]Department of Basic Sciences, College of Veterinary Medicine, Mississippi State University, Mississippi State, MS 39762

Running Head: *S. pneumoniae* metabolism altered by zinc-sensitive operon

Corresponding author: Justin A. Thornton, thornton@biology.msstate.edu

Abstract

Streptococcus pneumoniae colonizes the mucosa of the human nasopharynx and is a leading cause of community-acquired pneumonia, acute otitis media, and bacterial meningitis. Metal ion homeostasis is vital to the survival of this pathogen and contributes significantly to both colonization and invasive disease. Microarray and qRT-PCR analysis revealed an upregulation of an uncharacterized operon (*SP1433-1438*) in pneumococci subjected to metal-chelation by *N*,*N*,*N*',*N*' -tetrakis-(2-Pyridylmethyl)ethylenediamine (TPEN). Supplementation of either zinc or cobalt following TPEN treatment drastically abrogated induction. BLAST analysis predicted this operon to encode two ABC-transporters, sharing homology to a multidrug resistance system (SP1434-1435) and an energy-coupling factor (ECF) transport system (SP1436-1438). Inductively coupled plasma mass spectrometry (ICP-MS) analysis indicated changes in intracellular concentrations of iron, zinc, and manganese ions in a Δ1434-8 strain compared to parental T4R. Analysis of the secreted metabolomic profile of the T4R and Δ1434-8 strains identified significant changes in pneumococcal glycolytic pathways, indicating a shift towards increased production of acetate. Additionally, proteomic analysis revealed 41 differentially expressed proteins in the Δ1434-8 strain, with roughly 20% of them regulated by the global catabolite repressor, CcpA. Based on these findings, we propose that the *SP1433-1438* operon is largely involved in the central metabolism of *S. pneumoniae* during zinc-limitation.

Importance

Metal sequestration is a common strategy utilized by the host immune response as well as antibiotics such as vancomycin to kill invading bacterial pathogens (1). However, pneumococcus is still able to thrive under zinc-limiting conditions. This study describes a previously uncharacterized operon encoding two ABC transport systems that are strongly

47 induced during zinc-limiting conditions. This operon was found to be regulated by a zinc-
48 dependent regulator (*SP1433*) that functions independently of the overarching AdcR regulon.
49 We have additionally utilized a 2D-NMR approach to analyze the secreted metabolome and
50 have employed proteomic analysis to identify a role for these systems in the maintenance of
51 cellular metabolism. This study provides new information on how *Streptococcus pneumoniae*
52 responds and adapts to zinc-limiting conditions.

53

54 **Introduction**

55 Bacteria have evolved a wide variety of ATP-binding cassette (ABC) transporters that
56 function primarily to transport molecules across cell membranes (2). These systems are
57 involved in the uptake and efflux of many substrates, including vitamin B12, iron-binding
58 siderophores, and free metal ions (3-5). These transport systems consist of importers, found
59 only in prokaryotic systems (types I, II, and III), and exporters, found in both prokaryotic and
60 eukaryotic systems (2). Type III importers, or energy coupling factor (ECF) transporters, were
61 the most recently characterized, and they differ from importer types I and II in that they lack
62 substrate-binding domains or proteins (6). ECF transporters are involved in the uptake of
63 vitamins (thiamine and riboflavin) and metal ions (cobalt and nickel) (7-9).

64

65 In an effort to starve bacterial pathogens of essential metals, the human immune
66 system expresses proteins that sequester metal ions, a process termed “nutritional immunity”
67 (10). As organisms continue to evade the immune response and evolve resistance to antibiotics,
68 metal homeostasis is an attractive target for future therapeutics. Discerning the mechanisms by
69 which pathogens respond to and overcome metal starvation is key to understanding the
70 physiology of the organism and developing novel therapeutics to eliminate them.

Streptococcus pneumoniae, pneumococcus, is a Gram-positive commensal of the human nasopharynx and is the leading cause of community acquired pneumonia worldwide (11). Zinc transport systems and the zinc-dependent AdcR regulon of the pneumococcus have been characterized in detail (12-15). However, it remains unknown if other zinc-sensitive transporters exist. Previous work from our laboratory has identified roles for zinc homeostasis in both invasion and biofilm formation of *S. pneumoniae* (12, 16). Here we identify zinc as an effector molecule for the regulation of a genetic locus involved in maintenance of metal homeostasis. We hypothesize that this locus encodes an operon that is zinc-sensitive and largely contributes to cellular metabolism, specifically relating to oxidative stress, carbohydrate metabolism, and metal ion uptake. Additionally, this study has utilized 2D NMR metabolomics and proteomic analysis to identify metabolic pathways of *Streptococcus pneumoniae* that contribute to homeostasis during zinc-stress.

Results

Prediction of Two Uncharacterized ABC-Transporters in Streptococcus pneumoniae

Microarray data of *Streptococcus pneumoniae* strain TIGR4 exposed to the zinc-chelator *N,N,N',N'*-tetrakis-(2-pyridylmethyl)ethylenediamine (TPEN) identified the gene loci *SP1434-1438* as some of the most highly upregulated genes in response to zinc-limitation (Supplemental Table 1). Due to their proximity to each other in the genome (Fig. 1A), and their similar response to zinc-chelation, we hypothesized that these genes comprise an operon involved in homeostasis during zinc-limitation. Analysis using the Database of prOkaryotic OpeRons (DOOR) supported our hypothesis that these genes are located within an operon (17). Co-regulation of genes *SP1434-1438* was verified by detecting a significant upregulation of

each gene by quantitative real time PCR (qRT-PCR) following zinc-chelation with TPEN (data not shown). InterPro analysis identified SP1434 and SP1435 as ABC transporter ATP-binding proteins, and BLAST analysis identified both SP1434 and SP1435 as multidrug resistance-like ATP-binding proteins (mdlB) (Supplemental Table 2). Though SP1434 and SP1435 were proposed to be involved in antibiotic efflux (18), when tested against a broad panel of antibiotics, a mutant strain lacking *SP1434* was equally as sensitive as the parental T4R (Supplemental Figure 1). SP1434 (orange) and SP1435 (red) are predicted to form an independent system with each protein containing five alpha helix transmembrane domains and a P-loop ATPase domain (Fig. 1B). Additionally, InterPro analysis indicated SP1436 as a conserved integral membrane protein, SP1437 as a membrane protein, and SP1438 as a cobalt(II) ABC transporter permease. BLAST analysis indicated that SP1436, SP1437, and SP1438 share sequence homology with components of an energy coupling factor (ECF) transport system, representing the substrate-specific component (EcfS), the transmembrane transporter component (EcfT), and the ATP-binding protein (EcfA2), respectively. The predicted ECF transport system is also shown, whereby, SP1436 (purple) binds the substrate, SP1437 (green) functions as a permease, and SP1438 (blue) acts as an ATPase utilizing energy generated by ATP hydrolysis to import the substrate into the cell.

Metal Availability Alters Expression of SP1434

To verify the microarray results, expression of the first gene in the operon (*SP1434*) was analyzed by qRT-PCR following TPEN treatment. Results from the qRT-PCR analysis indicated robust expression in response to the zinc(II) chelation, as *SP1434* was upregulated greater than 100-fold in comparison to a control sample without TPEN treatment (Fig. 2). In contrast, expression of *SP1434* was unaltered in samples exposed to excess metal ion concentrations; addition of zinc ions led to a 0.7-fold change and adding cobalt(II) (-1.3), iron(II) (-1.1), and

nickel(II) (-1.1) yielded similar results. To determine individual metals' effect on chelation-dependent operon expression, samples were treated with TPEN for 15 min followed by supplementation with excess metal for 15 min. Surprisingly, addition of zinc or cobalt ions limited the upregulation of *SP1434* by roughly 90 %, and nickel(II) limited expression by 30% compared to a control treated only with TPEN for 30 min. However, addition of iron(II) following TPEN treatment limited upregulation by less than 10%. This is important to note as TPEN, in addition to binding zinc(II) at a 1:1 ratio (K_d = 2.6 × 10^{-16} M), also has an affinity for iron(II) (K_d = 2.4 × 10^{-15} M) (19). Collectively, these data indicate this system is responsive to multiple divalent metal ions, but it does not appear to be affected by iron availability.

Transcriptional Regulation of SP1434-1438 Operon

The locus directly upstream of *SP1434* encodes a previously uncharacterized AraC transcriptional regulator (*SP1433*). To determine if *SP1433* is involved in the induction of *SP1434* following TPEN treatment, expression of *SP1433* and *SP1434* were assessed by qRT-PCR in the parental T4R and a Δ1433 mutant strain. Expression of *SP1433* in the T4R strain following TPEN treatment revealed an upregulation of ≈7 fold (Fig. 3). As expected expression of *SP1433* was undetectable in the Δ1433 mutant. Though *SP1434* was strongly upregulated following TPEN exposure in the T4R strain, expression of *SP1434* did not increase following treatment with TPEN in the Δ1433 mutant strain. These data indicate involvement of *SP1433* in the regulation of this operon. To identify if *SP1433* falls within the previously characterized AdcR zinc-dependent regulon, expression of genes known to be regulated by AdcR, *adcA* and *adcAII*, were analyzed in T4R and the Δ1433 mutant. However, no significant differences in expression of *adca* or *adcAII* were detected between the two strains (Supplemental Figure 2), indicating that while the *SP1434-1438* operon is regulated by *SP1433* and is highly responsive to metal-starvation, it is unlikely part of the AdcR regulon and is instead an independent metal sensor.

SP1434-1438 Alters Intracellular Metal Availability

The considerable upregulation of this operon following zinc chelation led us to investigate the intracellular metal ion concentrations within T4R and the Δ1434-8 strain using inductively coupled plasma mass spectrometry (ICP-MS). These analyses revealed significant differences in intracellular manganese(II), iron(II), and zinc(II) concentrations, between the two strains (Fig. 4, Supplemental Table 4). Due to sequence similarity with a cobalt/nickel ECF transport system, the difference in intracellular nickel(II) concentration is interesting to note though this was not statistically significant under the conditions tested.

Secreted Metabolome of T4R and Δ1434-8

Metals have been shown to impact bacterial metabolism, and a recent study of *Streptococcus pyogenes* showed that excess zinc ions interfere in glucose metabolism through the inhibition of two enzymes: phosphofructokinase and glyceraldehyde-3-phosphate-dehydrogenase (20). To determine the role that the *SP1434-1438* operon is playing in metabolism, potentially due to intracellular metal accumulation, secreted metabolomics were performed on both T4R and Δ1434-8 using a novel 2D nuclear magnetic resonance (NMR) approach. Briefly, cultures of each strain were grown to early log (OD_{600} 0.2), mid-log (OD_{600} 0.35) and beginning stationary phase (OD_{600} 0.5). Culture supernatants were sterile filtered, processed, and quantified by NMR, using a library containing more than fifty metabolites. Partial Least Squares Discriminant Analysis (PLS-DA) of these samples detected significant differences in metabolite concentrations both between strains of pneumococci and across the different optical densities analyzed (Fig. 5A). In addition to identifying the collective differences between strains, significant differences were also detected in individual metabolites between

169 strains, including lactate, acetate, and carbohydrates (Fig. 5B); however, differences were also
170 detected in numerous amino acids including threonine, arginine, and cysteine. A heatmap
171 identifying differences between the two strains throughout the time course of the experiment
172 and clustering metabolites with similar behavior is shown in Supplemental Figure 3. Broadly, the
173 metabolites fall into two main classes: compounds that rapidly increase as OD_{600} increases,
174 including L-cystine, threonine, and lactic acid, and compounds which decrease over time.
175 Additionally, metabolic pathways were mapped showing the most significantly altered
176 metabolites of both T4R and Δ1434-8, with the most metabolic changes occurring during
177 pyruvate metabolism (Fig. 5C). Collectively, these data indicate involvement of this operon in
178 the regulation of cellular metabolism, particularly in glucose and amino acid metabolism.
179

180 ***Proteomic Analysis of T4R and Δ1434-8***

181 To identify potential mechanisms leading to differences in the metabolic profiles between
182 T4R and Δ1434-8 strains, proteomic analysis of both T4R and Δ1434-8 were performed using
183 mass spectrometry-based methods. Using a Fisher's exact t-test ($p < 0.003$), we identified 41-
184 differentially expressed proteins in the Δ1434-8 strain compared to the parental T4R (Table 1).
185 Differentially expressed proteins were analyzed through KEGG, STRING, Uniprot, and
186 RegPrecise to determine potentially relevant metabolic and regulatory pathways (21-24). From
187 these data, roughly 22% of those differentially expressed, fall within the CcpA, global catabolite
188 repression regulon (25, 26). Two of the 41 differentially expressed proteins fall under the
189 regulation of CodY, which is also a known global nutritional regulator (27). In addition to the
190 CcpA and CodY regulons, multiple differentially expressed proteins were identified as belonging
191 to the ArgR, the predicted-Rex, and the CtsR regulons, indicating changes in arginine
192 metabolism and redox stimuli between the Δ1434-8 strain and parental T4R (28-31).

193 Furthermore, expression of ABC-transporters or phosphotransferase systems accounted for
194 more than 20% of the downregulated proteins in the Δ1434-8 strain.
195

196 **Discussion**

197 *Streptococcus pneumoniae* remains one of the leading killers of children worldwide, and
198 infections due to this organism account for more than 400,000 hospitalizations per year in the
199 United States alone (32). The pneumococcus primarily resides as a commensal of the
200 nasopharynx, where zinc(II) concentrations are limited. Additionally, exposure to calprotectin, a
201 protein produced by neutrophils to sequester zinc ions from bacteria, further limits metal
202 availability within the host. Pathogens must therefore utilize mechanisms to circumvent metal
203 starvation. Though zinc(II) acquisition and regulation have been well characterized in *S.*
204 *pneumoniae*, in this study we have identified a previously uncharacterized system that is
205 strongly responsive to zinc-limitation. Furthermore, loss of this genetic locus results in an altered
206 cellular metabolism. Our results indicate that genes *SP1433-1438* are encoded as an operon
207 that is highly upregulated in response to zinc-chelation by the cell permeable chelator, TPEN,
208 potentially mimicking the environment encountered during neutrophil clearance in the human
209 nasopharynx. BLASTp and UniProt analysis revealed the potential of this operon to encode two
210 transport systems sharing homology to an antibiotic transport system and a cobalt(II)/nickel(II)
211 energy coupling factor transport system. *SP1434* and *SP1435* of this system were recently
212 characterized to be involved in pneumococcal environmental information processing and were
213 found to be highly responsive following deletion of the two-component regulatory system 08
214 (TCS08) histidine kinase (33). Moreover, the pneumococcal TCS08 has shown to be
215 homologous to the SaeRS system of *Staphylococcus aureus* that is activated by calprotectin,
216 further suggesting the involvement of this system to metal limitation (34, 35).
217

Due to the promiscuous metal-binding affinity of TPEN, we investigated the effect of other metals on expression of *SP1434*. This operon was determined to be responsive to zinc, cobalt, and nickel ions, as supplementation following TPEN treatment led to a drastic limitation in the upregulation of *SP1434* seen in TPEN treated samples alone. Additionally, we detected upregulation of *SP1434* in the parental T4R strain but no increase in expression in the strain lacking the AraC transcriptional regulator (Δ1433), indicating *SP1433* as the regulator of this operon. Expression of AdcR-regulon genes *adcA* and *adcAII* encoding zinc-binding lipoproteins were not affected in the Δ1433 strain, suggesting that *SP1433* is likely a zinc-sensing regulator functioning independently of AdcR.

Since components of this operon share sequence similarity with metal ion transport systems, we analyzed intracellular metal concentrations of T4R and Δ1434-8 by intercoupled plasma-mass spectrometry (ICP-MS). Significant differences were detected in the concentrations of manganese, zinc, and iron ions. Iron(II) is known to interact with H_2O_2 through Fenton chemistry to form highly reactive hydroxyl radicals (36), whereas zinc and manganese are known to function as antioxidant metal ions specifically through redox-active metal antagonism and interaction with the superoxide dismutase, SodA (37, 38). As metal ions are also known to be important enzymatic cofactors for proteins involved in metabolism, and H_2O_2 is a significant byproduct of pneumococcal metabolism, we explored how loss of this operon, and subsequent changes in intracellular metal ion concentrations, altered cellular metabolism. NMR-based metabolomics of culture supernatants identified major shifts in the metabolic profiles between strains, primarily with increased production of lactate in the T4R strain and increased production of acetate in the Δ1434-8 strain. These differences suggest a preference for mixed acid fermentation by Δ1434-8 versus homolactic acid fermentation by the T4R strain (39). Several amino acids were also observed to exhibit differing metabolite behavior. Of particular interest were the high levels of cysteine detected in Δ1434-8 strain since this strain contains

244 higher concentrations of zinc(II) and cysteine residues are known to interact with zinc ions with
245 high affinity (40).
246
247 Proteomic analysis validated the results obtained from the secreted metabolomics and
248 indicated that nearly one quarter of differentially expressed proteins were regulated by the CcpA
249 regulon, involved in carbohydrate catabolite repression. The CcpA regulon has been previously
250 characterized as a master regulator that controls fermentation, as well as catabolism of glucose,
251 galactose, and tagatose (26). Many of the differentially expressed proteins that fall within the
252 CcpA regulon were downregulated and are known to be involved in galactose fermentation,
253 including GatB and the *nan* operon (41, 42). Additionally, CcpA regulation is thought to be
254 important for host interactions and contributes to successful colonization (26, 43). Previous
255 studies have linked sialic acid and CcpA with galactose metabolism specifically through the
256 pneumococcal *nan* operons(42), and it is therefore interesting to note that 4/5 of the genes
257 within this operon in the D39 background (*spd_1263*, *spd_1264*, *spd_1265*, and *spd_1267*)
258 were found to be upregulated when grown with 0.5% sialic acid) (42).
259
260 In addition to the large number of genes that were identified within the CcpA regulon,
261 results from our proteomic analysis also detected differential expression of proteins within the
262 CodY, ArgR, and Rex regulons. CodY has been shown to be involved in the regulation of
263 colonization and amino acid metabolism and could potentially drive the amino acid differences
264 observed in our metabolomic analyses (44). Arginine metabolism has been linked to virulence in
265 *Streptococcus pneumoniae* and other significant human pathogens and it is interesting to note
266 that one of the six proteins detected to be upregulated in our proteomic analysis was an arginine
267 transport system that is regulated by the ArgR regulon (28). The Rex (redox-sensing regulator)
268 regulon detected by RegPrecise has been characterized in both *Streptococcus mutans* and
269 *Staphylococcus aureus*, though to our knowledge has not yet been characterized in *S.*

pneumoniae (45, 46). In both *S. mutans* and *S. aureus* Rex has been shown to sense NAD^+ or NADH, and in *S. aureus* Rex is thought to be the central regulator of anaerobic metabolism (46). Findings from our proteomics analyses indicate that the involvement of Rex in this system is at the level of a zinc(II) and iron(II)-binding alcohol dehydrogenase, both of which are also under the regulation of CcpA. An additional protein thought to be under coregulation by Rex and CodY that was identified in our proteomics data is a glyceraldehyde-3-phosphate-dehydrogenase. Collectively, these data indicate major metabolic differences between our T4R strain and the Δ1434-8 strain, particularly in carbohydrate metabolism, fermentation, and amino acid metabolism.

In this study, we identified a previously uncharacterized operon of *Streptococcus pneumoniae* that is strongly responsive to zinc-chelation, yet independent of the AdcR zinc(II) regulon. We have identified the regulator for this genetic locus and have determined that mutants lacking the operon (Δ1434-8) display different intracellular metal ion ratios and altered metabolic profiles. Analysis of the secreted metabolomes and proteomic profiles suggest changes in central carbohydrate metabolism, potentially through a shift in fermentation pathways. These data demonstrate that the metabolome of *Streptococcus pneumoniae* is largely metal-dependent, which to our knowledge has not yet been characterized. This work provides a foundation for identifying key metabolic enzymes and intermediates that could be targeted using metal-dependent therapeutics.

Materials and Methods

DNA Manipulation

S. pneumoniae strains TIGR4 and its unencapsulated mutant (T4R) were grown on tryptic soy agar plates supplemented with 5% defibrinated sheep blood or in C+Y medium. Mutants of TIGR4 and T4R lacking *SP1434-1438* (Δ1434-8) and SP1433 (Δ1433) were created using splicing by overlap extension (SOE) PCR method using an erythromycin or spectinomycin antibiotic cassette and standard *S. pneumoniae* transformation procedures. Mutants lacking SP1434-1438 and SP1433 were isolated by selection on blood agar plates supplemented with erythromycin (0.5 µg/mL) or spectinomycin (500 µg/mL), respectively, and confirmed by PCR.

Antibiotic Sensitivity

Frozen bacterial stocks of T4R and Δ1434-8 were diluted to $1x10^7$ CFU/mL and 100 µL were spread on a blood agar plate. Discs impregnated with antibiotics at the following amounts were added to blood agar plates and were incubated overnight at 37 ˚C with 5% CO_2 (Ciprofloxacin 5 µg, Vancomycin 30 µg, Ampicillin 10 µg, Penicillin 10 U, Ceftiofur 30 µg, Cephalothin 30 µg, and Sulfisoxazole 1 mg). Following incubation, zones of inhibition surrounding antibiotic discs were measured.

Inductively Coupled Plasma Mass Spectrometry

Bacterial cultures of T4R and Δ1434-8 were grown to $OD_{600\ nm}$ 0.6 in triplicate. Four 1 mL cultures were collected of each strain, centrifuged at 16,000xg for 5 min, and supernatant was decanted. Pellets were heat killed at 65 ˚C for 2 hr. Pellets were resuspended in 100 µL

313 concentrated nitric acid, then were diluted 1:20 with water. An Agilent ICP-MS 7500cx was used
314 to collect all ICPMS data herein.
315

316 ***Quantitative Real-time PCR***

317 For assays investigating *SP1434* expression, *S. pneumoniae* T4R was grown in C+Y
318 medium to $O.D._{600\ nm}$ of 0.6 prior to the addition of the Zn^{2+}-chelating agent TPEN (30 µM) or
319 zinc(II), cobalt(II), iron(II), or nickel(II) ions at 200 µM. Supplemented metals were TraceCERT®
320 ICP-MS grade (Sigma-Aldrich). After addition of TPEN or individual metals, bacteria were
321 incubated at 25°C for 15 min. Additionally, cultures were exposed to TPEN for 15 min followed
322 by metal for a following 15 min. For assays investigating *SP1433* expression, T4R and Δ1433
323 were grown to $O.D._{600\ nm}$ of 0.6 and treated for 15 min with TPEN (30 µM). For all samples, after
324 incubation, 1 mL of bacterial culture was added to 2 mL of RNAprotect (Qiagen). Samples were
325 incubated at room temperature for 5 min. Two mL of bacterial culture in RNAprotect was
326 pelleted for 5 min at 16,000xg, pellets were resuspended in 1 mL of cold RNase free PBS and
327 centrifuged again. Supernatants were decanted, and pellets were resuspended in 400 µL RLT
328 buffer (Qiagen) with 2-mercaptoethanol (Sigma-Aldrich). Samples were sonicated three times
329 (15 sec), 600 µL RLT buffer was added to each sample, and samples were transferred to 500
330 µL of 0.7 mM Zirconia beads. Samples were bead beat for 2 min using Mini-BeadBeater 16
331 (BioSpec Products). Lysates were centrifuged on tabletop centrifuge at 2,000xg for 1 min.
332 Samples were run through Qiashredder columns (Qiagen) per manufacturer's instructions.
333 100% Ethanol was added to Qiashredder flow through at 0.6 volume of the sample. RNA was
334 purified using a Qiagen RNeasy Mini Kit (Qiagen), optional on-column DNase treatment was
335 performed for 30 min, RNA was then quantitated using a Qubit, and 5 ng of each sample was
336 used to synthesize cDNA using a Maxima First Strand cDNA synthesis kit (Thermo Scientific).
337 cDNA products were diluted 1:10 and 1 µL of cDNA was used as template for qRT-PCR using

338 Luminaris Color HiGreen High ROX qPCR Master Mix (Thermo Scientific) per manufacturer's
339 instructions. Primer sequences can be found in Supplemental Table 3.

340

341 ***Secreted Metabolomics***

342 Cultures of T4R and Δ1434-8 were grown to $OD_{600\ nm}$ 0.2, 0.35 and 0.5. One milliliter of
343 culture was removed and centrifuged at 16,000xg for 5 min and sampling was performed in
344 triplicate. Culture supernatants were then filtered using 0.22 µM filters. NMR samples were made
345 by combining the filtered supernatant (400 µL) with 200 µL of 200 mM phosphate buffer (pH 7.0)
346 with 1.000 mM trimethylsilypropanoic acid (TMSP) in 50% D_2O. The 1D and 2D NMR spectra
347 were obtained at a temperature of 298 K on a 600 MHz Bruker Avance III cryoprobe equipped
348 NMR spectrometer. A 1D-NOESY (noesypr1d) pulse sequence was used, and presaturation
349 applied at 4.75 ppm during the 4 second relaxation delay and 50 millisecond mixing time to
350 suppress the water signal. A 1 second acquisition time was used, and a total of 64 scans were
351 collected with a 20-ppm spectral width. A modified 2D-TOCSY (dipsi2gpphzsprespe_psyche)
352 pulse sequence was used for 2D acquisition. This sequence incorporated broadband
353 homonuclear decoupling using PSYCHE in the t_1 dimension(47-49). A zero-quantum filter was
354 used during the 80 ms TOCSY mixing time. Water flip back pulses were used to optimize water
355 suppression (50). Each FID was collected using 2 scans, and the indirect dimension was sampled
356 for 85 ms using 1024 complex points. Additional water suppression and solvent filtering were
357 performed with NMRPipe using in-house scripts (51). Each spectrum was calibrated using the
358 TMSP peak as an internal standard and manually processed. Compounds in the processed
359 spectra were identified and quantified using AMIX-Viewer v3.9.14 software (Bruker Biospin
360 GmbH). A library of 56 pure compounds at 3.000 mM was created in-house to identify and quantify
361 peak intensities and line widths for each compound. The output file from AMIX was a listing of

362 concentration for each compound for each sample. Concentrations for each sample (T4R and Δ
363 1434-8) and O.D. (0.2, 0.35 and 0.5) were used for the statistical analysis.
364
365 The metabolite concentrations for each sample was arranged by O.D. values and strain
366 before the statistical analysis was conducted using MetaboAnalyst(52). MetaboAnalyst
367 normalized the samples by sum with Pareto scaling. The Pareto scaling was used to emphasize
368 the weaker metabolites and reduce the influence of the intense peaks to easily identify the
369 biological relevance(53). After normalization, the statistical methods, such as multivariate
370 analysis, were used for data analysis. The PLS-DA data set was divided into components to
371 identify the statistical differences between the classes. The first component (Component 1)
372 captured the maximum variance in the data set that was the linear combination of the original
373 predictor variables compared to the observed variables, whereas the other components (second,
374 third, fourth, etc.) captured the remaining variance in the data set that was the linear combination
375 and orthogonal to the first component(53).
376

377 ***Proteomic Analysis***

378 Four cultures of T4R and Δ1434-8 were grown to $OD_{600\ nm}$ 0.4 in C+Y medium and
379 subjected to liquid chromatography-tandem mass spectrometry (LC-MS/MS) analysis as
380 previously described (54, 55). Briefly, proteins were isolated from bacterial pellets sonicated in
381 NP-40 lysis buffer (0.5% NP-40, 150 mM NaCl, 20 mM $CaCl_2 \cdot 2H_2O$, 50 mM Tris, pH 7.4)
382 supplemented with protease inhibitor cocktail (c0mplete™, Sigma-Aldrich) using a Covaris S220
383 focused-ultrasonicator. Protein concentration was determined using Thermo Scientific Pierce
384 BCA Protein Assay Kit. Precipitation of 30 µg of protein was performed with methanol and
385 chloroform (4:1), solubilized in 8 M urea, reduced (5 mM dithiothreitol (DTT) at 65 ˚C for 10 m)
386 and alkylated (0.01 M iodoacetamide at 37 ˚C for 30 m) and digested with porcine trypsin (at 37

387 ˚C, overnight, 50:1 ratio of protein. Tryptic peptides were desalted using a C18 spin column
388 (Thermo Fisher Scientific) and analyzed by linear trap quadropole (LTQ) Orbitrap Velos mass
389 spectrometer equipped with an Advion nanomate electrospray ionization (ESI) source (Advion).
390 Peptides (500 ng) were eluted from a C18 column (100 µm id × 2 cm) onto an analytical column
391 (75 µm ID × 10 cm, C18) using a 180 m gradient with 99.9% acetonitrile, 0.1% formate at a flow
392 rate of 400 nL/m and introduced into an LTQ-Orbitrap.

393

394 Data dependent scanning was performed by the Xcalibur v 2.1.0 software using a survey
395 mass scan at 60,000 resolution in the Orbitrap analyzer scanning mass/charge (m/z) 400–1600
396 followed by collision-induced dissociation (CID) tandem mass spectrometry (MS/MS) of the 14
397 most intense ions in the linear ion trap analyzer (56). Precursor ions were selected by the
398 monoisotopic precursor selection (MIPS) setting with selection or rejection of ions held to a ±10
399 ppm window. Dynamic exclusion was set to place any selected m/z on an exclusion list for 45 s
400 after a single MS/MS. Tandem mass spectra were searched against a *Streptococcus*
401 *pneumoniae* serotype 4 strain ATCC BAA/TIGR4 FASTA protein database downloaded from
402 UniProtKB to which common contaminant proteins (e.g., human keratins obtained at
403 ftp://ftp.thegpm.org/fasta/cRAP) were appended. All MS/MS spectra were searched using
404 Thermo Proteome Discoverer 1.3 (Thermo Fisher Scientific) considering fully tryptic peptides
405 with up to two missed cleavage sites. Variable modifications considered during the search
406 included methionine oxidation (15.995 Da), and cysteine carbamidomethylation (57.021 Da).
407 Peptides were identified at 99% confidence with XCorr score cutoffs based on a reversed
408 database search (57). The protein and peptide identification results were visualized with
409 Scaffold v 3.6.1 (Proteome Software Inc.). Protein identifications with a minimum of two
410 peptides identified at 0.1% peptide false discovery rate (FDR) were deemed correct. Significant
411 changes in protein expression between T4R and Δ1434-8 were identified by Fisher's exact test

412 at a p-value of ≤0.054 and fold change of ±1.3. Fold changes in protein expression were
413 calculated using weighted normalized spectra with 0.5 imputation value. Various bioinformatics
414 resources such as DAVID, KEGG, and STRING were utilized to determine the functions of the
415 identified proteins (22, 58, 59). The PRoteomics IDEntifications (PRIDE) database is a
416 centralized, standards compliant, public data repository for proteomics data. The mass
417 spectrometry proteomics data from this study is deposited to the ProteomeXchange Consortium
418 via the PRIDE partner repository (pending accession number) (60).

419

420 ***Statistics***

421 Intercoupled plasma mass spectrometry (ICP-MS), and H_2O_2 killing assays were
422 performed a minimum of three times, results from independent experiments were averaged
423 together, and standard error of the mean was calculated. Data sets were analyzed by
424 comparing parental T4R to Δ1434-8 using the students t-test, with an α value = 0.05. Results
425 were deemed statistically significant when p < alpha. Statistical analyses were performed using
426 GraphPad Prism 7.

427

428 **Acknowledgements**

429 Thank you to Allen Shack in the College of Basic Sciences and the staff of the Arizona
430 State University Mass Spectrometry Core for their assistance with the proteomic analysis
431 featured in the work presented here. This work was supported in part an Institutional
432 Development Award (IDeA) from the NIGMS COBRE grant number P20GM103646 (awarded to
433 JAT) and by a National Institutes of Health grant number R15GM113152 (awarded to NCF).

434

435

436 **Figure Legends**

437 **Figure 1. *SP1434-1438* Operon Model.** A) the genetic loci containing genes *SP1433-*
438 *SP1438* with the direction of transcription represented by the dotted arrow. Upstream of
439 this operon is an AraC transcriptional regulator, SP1433 (yellow). B) The working model
440 of the transporters encoded by genes *SP1434* (orange)-*SP1435* (red) and *SP1436-*
441 *SP1438* (purple, green, and blue, respectively).

442

443 **Figure 2. *SP1434* is highly zinc(II) sensitive.** Expression of *SP1434* measured by
444 qRT-PCR from RNA extracted following either 15 min treatment with zinc-chelator
445 TPEN (30 μM)/metals (200 μM) or 15 min TPEN (30 μM) exposure with additional 15
446 min metal supplementation. Fold changes were calculated by ΔΔCT analysis with *gyrA*
447 serving as internal control.

448

449 **Figure 3. AraC regulator (*SP1433*) regulates operon expression.** Gene expression
450 of *SP1433* and *SP1434* were assessed by qRT-PCR in T4R (black) and Δ*SP1433*
451 (gray) strain following 15 min treatment with TPEN (30 μM). Fold changes were
452 calculated by ΔΔCT analysis with *gyrA* serving as an internal control. Non-detectable
453 gene expression is represented by ND.

454

Figure 4. Intracellular metals of T4R and Δ1434-8. a) Metal content of T4R (black) and Δ1434-8 (gray) were assessed by inductively coupled plasma mass spectrometry (ICP-MS) and displayed as concentration in parts per billion (µg/L). Representative figure of three replicates, with bars indicating mean metal concentrations, and standard error of the mean represented by horizontal bars. *p <0.05 as determined by students t-test comparing T4R to Δ1434-8 strain for each individual metal analyzed.

Figure 5. Metabolic profile of T4R and Δ1434-8 A) Clustering of samples within the PLS-DA plot of T4R (blue) and Δ1434-8 (red) profiles indicate significant metabolic differences between the two strains at an $OD_{600\ nm}$ of 0.2, 0.35, and 0.5. B) PLS-DA VIP Scores plot of T4R and Δ1434-8 indicates the most significant metabolites identified between strains. C) Extracellular metabolite concentrations of T4R (blue) and Δ1434-8 (red) arranged in metabolic pathways.

Table 1. Differentially expressed proteins in ΔSP1434-8 versus T4R. Mass spectrometry based proteomic analysis of Δ1434-8 strain compared to the parental T4R from cultures grown to $OD_{600\ nm}$ 0.5 identified 41-differentially expressed proteins. Fisher's exact t-test p<0.00274. Highlighted colors represent regulons the proteins are fall within: CcpA (yellow), CodY (blue), Rex (red), CtsR (green), and ArgR (purple).

Supplemental Table 1. RNA was harvested from bacterial cultures of TIGR4 and TIGR4 treated with TPEN grown to $OD_{600\ nm}$ 0.5 and was used to synthesize cDNA for hybridization to pneumococcal microarray.

Supplemental Table 2. Blast analysis of S*. pneumoniae* TIGR4 proteins SP1433-SP1438 revealed homology to a transcriptional regulator and two transport systems.

Supplemental Table 3. Primers sequences used in this study for molecular cloning and gene expression studies by qRT-PCR.

Supplemental Figure 1. Antibiotic sensitivity of T4R and ΔSP1434-8. T4R (black) and ΔSP1434-8 (gray) were inoculated onto blood agar plates and antibiotic impregnated discs were added at the following concentrations: Ciprofloxacin 5 µg, Vancomycin 30 µg, Ampicillin 10 µg, Penicillin 10 U, Ceftiofur 30 µg, Cephalothin 30 µg, and Sulfisoxazole 1 mg. Following overnight incubation, zones of inhibition surrounding antibiotic discs were measured (mM).

Supplemental Figure 2. SP1433 specifically regulates SP1434-8. Gene expression of *adcAII*, *adcA*, *SP1434* and *SP1433* were assessed by qRT-PCR in T4R (black) and Δ*SP1433* (gray) strain following 15 min treatment with TPEN (30 µM). Fold changes

were calculated by ΔΔCT analysis with *gyrA* serving as an internal control. Non-detectable gene expression is represented by ND.

Supplemental Figure 3. Heatmap of secreted 2D-NMR metabolomics. Cultures of T4R and Δ1434-8 were grown to $OD_{600\ nm}$ 0.2, 0.35, 0.5. Supernatants were collected, sterile filtered, and analyzed against a metabolite library.

Supplemental Table 4. Mean intracellular metal ion concentrations in ppb (µg/L) in both the T4R and Δ1434-8 strains with standard deviation shown in parenthesis.

References

1. Zarkan A, Macklyne HR, Truman AW, Hesketh AR, Hong HJ. 2016. The frontline antibiotic vancomycin induces a zinc starvation response in bacteria by binding to Zn(II). Scientific Reports 6:19602.
2. Ter Beek J, Guskov A, Slotboom DJ. 2014. Structural diversity of ABC transporters. Journal of General Physiology 143:419-435.
3. Borths EL, Poolman B, Hvorup RN, Locher KP, Rees DC. 2005. *In Vitro* functional characterization of BtuCD-F, the *Escherichia coli* ABC transporter for vitamin B12 uptake. Biochemistry 44:16301-16309.
4. Koster W. 2001. ABC transporter-mediated uptake of iron, siderophores, heme and vitamin B12. Research in Microbiology 152:291-301.
5. Claverys J-P. 2001. A new family of high-affinity ABC manganese and zinc permeases. Research in Microbiology 152:231-243.
6. Rodionov DA, Hebbeln P, Eudes A, ter Beek J, Rodionova IA, Erkens GB, Slotboom DJ, Gelfand MS, Osterman AL, Hanson AD, Eitinger T. 2009. A novel class of modular transporters for vitamins in prokaryotes. Journal of Bacteriology 191:42-51.
7. Erkens GB, Majsnerowska M, ter Beek J, Slotboom DJ. 2012. Energy coupling factor-type ABC transporters for vitamin uptake in prokaryotes. Biochemistry 51:4390-6.
8. Kirsch F, Eitinger T. 2014. Transport of nickel and cobalt ions into bacterial cells by S components of ECF transporters. Biometals 27:653-60.
9. Josts I, Almeida Hernandez Y, Andreeva A, Tidow H. 2016. Crystal structure of a group I energy coupling factor vitamin transporter S component in complex with its cognate substrate. Cell Chemical Biology 23:827-36.

10. Weinberg ED. 1975. Nutritional immunity. Host's attempt to withold iron from microbial invaders. Journal of the American Medical Association 231:39-41.
11. CDC. 2015. Active Bacterial Core Surveillance Report, Emerging Infections Program Network, *Streptococcus pneumoniae*.
12. Brown LR, Gunnell SM, Cassella AN, Keller LE, Scherkenbach LA, Mann B, Brown MW, Hill R, Fitzkee NC, Rosch JW, Tuomanen EI, Thornton JA. 2016. AdcAII of *Streptococcus pneumoniae* affects pneumococcal invasiveness. PLOS ONE 11:e0146785.
13. Plumptre CD, Eijkelkamp BA, Morey JR, Behr F, Counago RM, Ogunniyi AD, Kobe B, O'Mara ML, Paton JC, McDevitt CA. 2014. AdcA and AdcAII employ distinct zinc acquisition mechanisms and contribute additively to zinc homeostasis in *Streptococcus pneumoniae*. Molecular Microbiology 91:834-51.
14. Bayle L, Chimalapati S, Schoehn G, Brown J, Vernet T, Durmort C. 2011. Zinc uptake by *Streptococcus pneumoniae* depends on both AdcA and AdcAII and is essential for normal bacterial morphology and virulence. Molecular Microbiology 82:904-16.
15. Manzoor I, Shafeeq S, Afzal M, Kuipers OP. 2015. The regulation of the AdcR regulon in *Streptococcus pneumoniae* depends both on $Zn^{(2+)}$- and $Ni^{(2+)}$-Availability. Frontiers in Cellular and Infection Microbiology 5:91.
16. Brown LR, Caulkins RC, Schartel TE, Rosch JW, Honsa ES, Schultz-Cherry S, Meliopoulos VA, Cherry S, Thornton JA. 2017. Increased zinc availability enhances initial aggregation and biofilm formation of *Streptococcus pneumoniae*. Frontiers in Cellular and Infection Microbiology 7.
17. Mao F, Dam P, Chou J, Olman V, Xu Y. 2009. DOOR: a database for prokaryotic operons. Nucleic Acids Research 37:D459-D463.
18. Tocci N, Iannelli F, Bidossi A, Ciusa ML, Decorosi F, Viti C, Pozzi G, Ricci S, Oggioni MR. 2013. Functional Analysis of Pneumococcal Drug Efflux Pumps Associates the MATE DinF Transporter with Quinolone Susceptibility. Antimicrobial Agents and Chemotherapy 57:248-253.
19. Arslan P, Di Virgilio F, Beltrame M, Tsien RY, Pozzan T. 1985. Cytosolic Ca^{2+} homeostasis in ehrlich and yoshida carcinomas. A new, membrane-permeant chelator of heavy metals reveals that these ascites tumor cell lines have normal cytosolic free Ca^{2+}. Journal of Biological Chemistry 260:2719-2727.
20. Ong C-lY, Walker MJ, McEwan AG. 2015. Zinc disrupts central carbon metabolism and capsule biosynthesis in *Streptococcus pyogenes*. Scientific Reports 5.
21. Novichkov PS, Laikova ON, Novichkova ES, Gelfand MS, Arkin AP, Dubchak I, Rodionov DA. 2010. RegPrecise: a database of curated genomic inferences of transcriptional regulatory interactions in prokaryotes. Nucleic Acids Research 38:D111-D118.
22. Szklarczyk D, Morris JH, Cook H, Kuhn M, Wyder S, Simonovic M, Santos A, Doncheva NT, Roth A, Bork P, Jensen LJ, von Mering C. 2017. The STRING database in 2017: quality-controlled protein–protein association networks, made broadly accessible. Nucleic Acids Research 45:D362-D368.
23. Consortium U. 2015. UniProt: a hub for protein information, vol 43, p D204-D212.
24. Kanehisa M. 2002. The KEGG database. silico simulation of biological processes 247:91-103.
25. Iyer R, Baliga NS, Camilli A. 2005. Catabolite control protein A (CcpA) contributes to virulence and regulation of sugar metabolism in *Streptococcus pneumoniae*. Journal of Bacteriology 187:8340-8349.
26. Carvalho SM, Kloosterman TG, Kuipers OP, Neves AR. 2011. CcpA Ensures Optimal Metabolic Fitness of *Streptococcus pneumoniae*. PLOS ONE 6:e26707.
27. Caymaris S, Bootsma HJ, Martin B, Hermans PWM, Prudhomme M, Claverys J-P. 2010. The global nutritional regulator CodY is an essential protein in the human pathogen *Streptococcus pneumoniae*. Molecular Microbiology 78:344-360.

28. Kloosterman TG, Kuipers OP. 2011. Regulation of arginine acquisition and virulence gene expression in the human pathogen *Streptococcus pneumoniae* by transcription regulators ArgR1 and AhrC. Journal of Biological Chemistry 286:44594-44605.
29. Bitoun JP, Nguyen AH, Fan Y, Burne RA, Wen ZT. 2011. Transcriptional repressor Rex is involved in regulation of oxidative stress response and biofilm formation by Streptococcus mutans. FEMS Microbiol Lett 320:110-7.
30. Michel A, Agerer F, Hauck CR, Herrmann M, Ullrich J, Hacker J, Ohlsen K. 2006. Global Regulatory Impact of ClpP Protease of Staphylococcus aureus on Regulons Involved in Virulence, Oxidative Stress Response, Autolysis, and DNA Repair. Journal of Bacteriology 188:5783-5796.
31. Chastanet A, Prudhomme M, Claverys J-P, Msadek T. 2001. Regulation of Streptococcus pneumoniae clp Genes and Their Role in Competence Development and Stress Survival. Journal of Bacteriology 183:7295-7307.
32. CDC. 2016. The Pink Book.
33. Gómez-Mejia A, Gámez G, Hirschmann S, Kluger V, Rath H, Böhm S, Voß F, Kakar N, Petruschka L, Völker U, Brückner R, Mäder U, Hammerschmidt S. 2018. Pneumococcal metabolic adaptation and colonization is regulated by the two-component regulatory system 08. bioRxiv doi:10.1101/300095.
34. McKessar SJ, Hakenbeck R. 2007. The Two-Component Regulatory System TCS08 Is Involved in Cellobiose Metabolism of Streptococcus pneumoniae R6. Journal of Bacteriology 189:1342-1350.
35. Cho H, Jeong DW, Liu Q, Yeo WS, Vogl T, Skaar EP, Chazin WJ, Bae T. 2015. Calprotectin Increases the Activity of the SaeRS Two Component System and Murine Mortality during Staphylococcus aureus Infections. PLoS Pathog 11:e1005026.
36. Koppenol WH. 1993. The centennial of the Fenton reaction. Free Radical Biology and Medicine 15:645-651.
37. Powell SR. 2000. The antioxidant properties of zinc. J Nutr 130:1447s-54s.
38. Yesilkaya H, Kadioglu A, Gingles N, Alexander JE, Mitchell TJ, Andrew PW. 2000. Role of manganese-containing superoxide dismutase in oxidative stress and virulence of Streptococcus pneumoniae. Infect Immun 68:2819-26.
39. Hartel T, Eylert E, Schulz C, Petruschka L, Gierok P, Grubmuller S, Lalk M, Eisenreich W, Hammerschmidt S. 2012. Characterization of central carbon metabolism of *Streptococcus pneumoniae* by isotopologue profiling. Journal of Biological Chemistry 287:4260-74.
40. Pace NJ, Weerapana E. 2014. Zinc-binding cysteines: diverse functions and structural motifs. Biomolecules 4:419-434.
41. Bidossi A, Mulas L, Decorosi F, Colomba L, Ricci S, Pozzi G, Deutscher J, Viti C, Oggioni MR. 2012. A Functional Genomics Approach to Establish the Complement of Carbohydrate Transporters in Streptococcus pneumoniae. PLOS ONE 7:e33320.
42. Afzal M, Shafeeq S, Ahmed H, Kuipers OP. 2015. Sialic Acid-Mediated Gene Expression in Streptococcus pneumoniae and Role of NanR as a Transcriptional Activator of the nan Gene Cluster. Applied and Environmental Microbiology 81:3121-3131.
43. Al-Bayati FAY, Kahya HFH, Damianou A, Shafeeq S, Kuipers OP, Andrew PW, Yesilkaya H. 2017. Pneumococcal galactose catabolism is controlled by multiple regulators acting on pyruvate formate lyase. Scientific Reports 7:43587.
44. Hendriksen WT, Bootsma HJ, Estevão S, Hoogenboezem T, de Jong A, de Groot R, Kuipers OP, Hermans PWM. 2008. CodY of *Streptococcus pneumoniae*: link between nutritional gene regulation and colonization. Journal of Bacteriology 190:590-601.
45. Baker JL, Derr AM, Karuppaiah K, MacGilvray ME, Kajfasz JK, Faustoferri RC, Rivera-Ramos I, Bitoun JP, Lemos JA, Wen ZT, Quivey RG. 2014. *Streptococcus mutans* NADH oxidase lies at the

623 intersection of overlapping regulons controlled by oxygen and NAD+ levels. Journal of
624 Bacteriology 196:2166-2177.
625 46. Pagels M, Fuchs S, Pané-Farré J, Kohler C, Menschner L, Hecker M, McNamarra PJ, Bauer MC,
626 Von Wachenfeldt C, Liebeke M, Lalk M, Sander G, Von Eiff C, Proctor RA, Engelmann S. 2010.
627 Redox sensing by a Rex-family repressor is involved in the regulation of anaerobic gene
628 expression in *Staphylococcus aureus*. Molecular Microbiology 76:1142-1161.
629 47. Foroozandeh M, Adams RW, Meharry NJ, Jeannerat D, Nilsson M, Morris GA. 2014. Ultrahigh-
630 Resolution NMR Spectroscopy. Angewandte Chemie International Edition 53:6990-6992.
631 48. Foroozandeh M, Adams RW, Kiraly P, Nilsson M, Morris GA. 2015. Measuring couplings in
632 crowded NMR spectra: pure shift NMR with multiplet analysis. Chemical Communications
633 51:15410-15413.
634 49. Foroozandeh M, Adams RW, Nilsson M, Morris GA. 2014. Ultrahigh-Resolution Total Correlation
635 NMR Spectroscopy. Journal of the American Chemical Society 136:11867-11869.
636 50. Thrippleton MJ, Keeler J. 2003. Elimination of Zero-Quantum Interference in Two-Dimensional
637 NMR Spectra. Angewandte Chemie International Edition 42:3938-3941.
638 51. Delaglio F, Grzesiek S, Vuister GW, Zhu G, Pfeifer J, Bax A. 1995. NMRPipe: A multidimensional
639 spectral processing system based on UNIX pipes. Journal of Biomolecular NMR 6:277-293.
640 52. Xia J, Wishart DS. 2002. Using MetaboAnalyst 3.0 for Comprehensive Metabolomics Data
641 Analysis, Current Protocols in Bioinformatics doi:10.1002/cpbi.11. John Wiley & Sons, Inc.
642 53. Worley B, Powers R. 2013. Multivariate Analysis in Metabolomics. Curr Metabolomics 1:92-107.
643 54. Shah P, Nanduri B, Swiatlo E, Ma Y, Pendarvis K. 2011. Polyamine biosynthesis and transport
644 mechanisms are crucial for fitness and pathogenesis of *Streptococcus pneumoniae*. Microbiology
645 157:504-15.
646 55. Rai AN, Thornton JA, Stokes J, Sunesara I, Swiatlo E, Nanduri B. 2016. Polyamine transporter in
647 *Streptococcus pneumoniae* is essential for evading early innate immune responses in
648 pneumococcal pneumonia. Scientific Reports 6:26964.
649 56. Andon NL, Hollingworth S, Koller A, Greenland AJ, Yates JR, 3rd, Haynes PA. 2002. Proteomic
650 characterization of wheat amyloplasts using identification of proteins by tandem mass
651 spectrometry. Proteomics 2:1156-68.
652 57. Qian WJ, Jacobs JM, Camp DG, 2nd, Monroe ME, Moore RJ, Gritsenko MA, Calvano SE, Lowry SF,
653 Xiao W, Moldawer LL, Davis RW, Tompkins RG, Smith RD. 2005. Comparative proteome analyses
654 of human plasma following in vivo lipopolysaccharide administration using multidimensional
655 separations coupled with tandem mass spectrometry. Proteomics 5:572-84.
656 58. Huang da W, Sherman BT, Lempicki RA. 2009. Systematic and integrative analysis of large gene
657 lists using DAVID bioinformatics resources. Nature Protocols 4:44-57.
658 59. Yoshida M, Kashiwagi K, Kawai G, Ishihama A, Igarashi K. 2001. Polyamine enhancement of the
659 synthesis of adenylate cyclase at the translational level and the consequential stimulation of the
660 synthesis of the RNA polymerase ς28 subunit. Journal of Biological Chemistry 276:16289-16295.
661 60. Vizcaino JA, Csordas A, del-Toro N, Dianes JA, Griss J, Lavidas I, Mayer G, Perez-Riverol Y,
662 Reisinger F, Ternent T, Xu QW, Wang R, Hermjakob H. 2016. 2016 update of the PRIDE database
663 and its related tools. Nucleic Acids Research 44:D447-56.

664

A

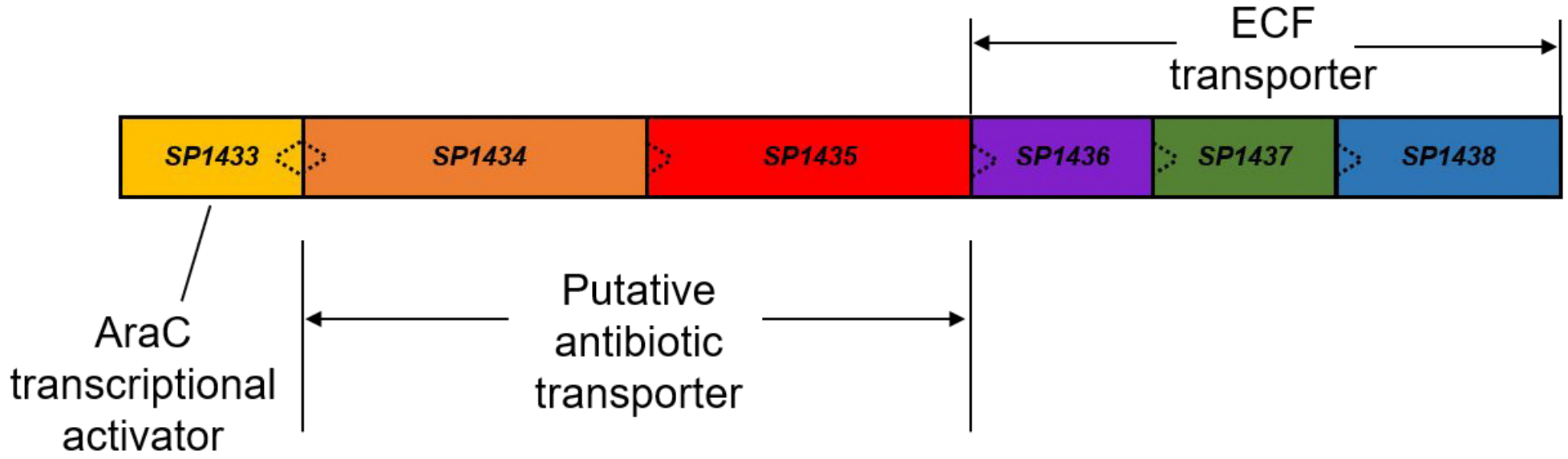
ECF
transporter
SP1433
SP1434
SP1435
SP1436
SP1437
SP1438
AraC
transcriptional
activator
Putative
antibiotic
transporter

B

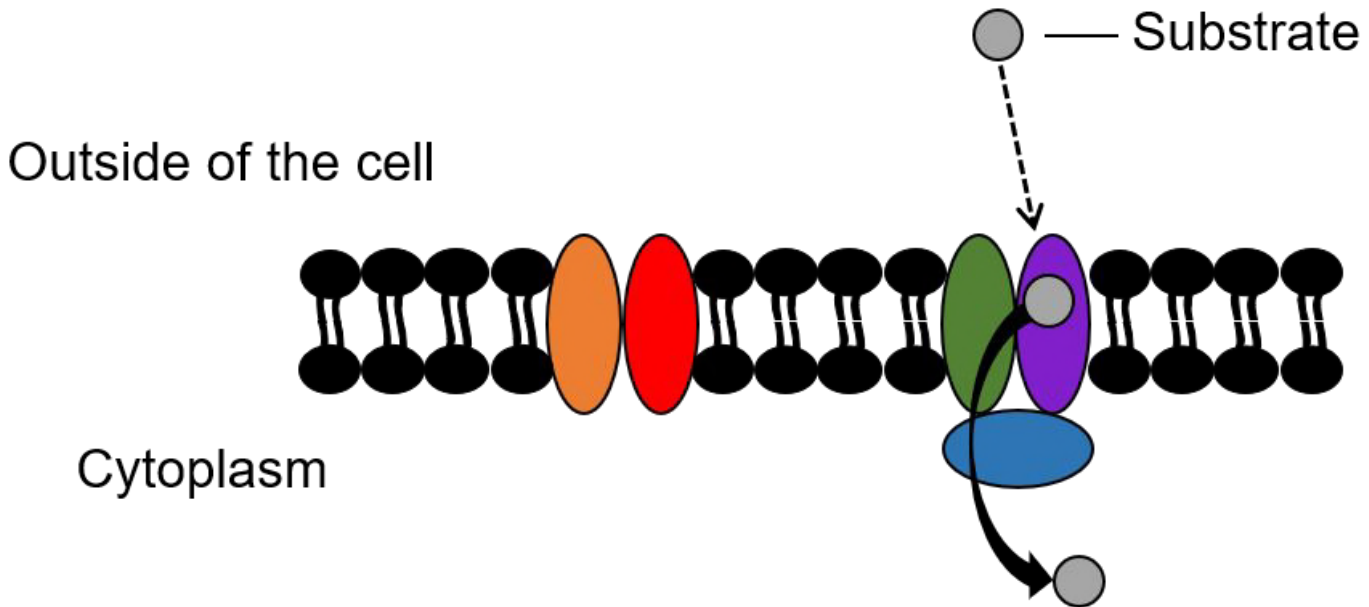
Substrate
Outside of the cell
Cytoplasm

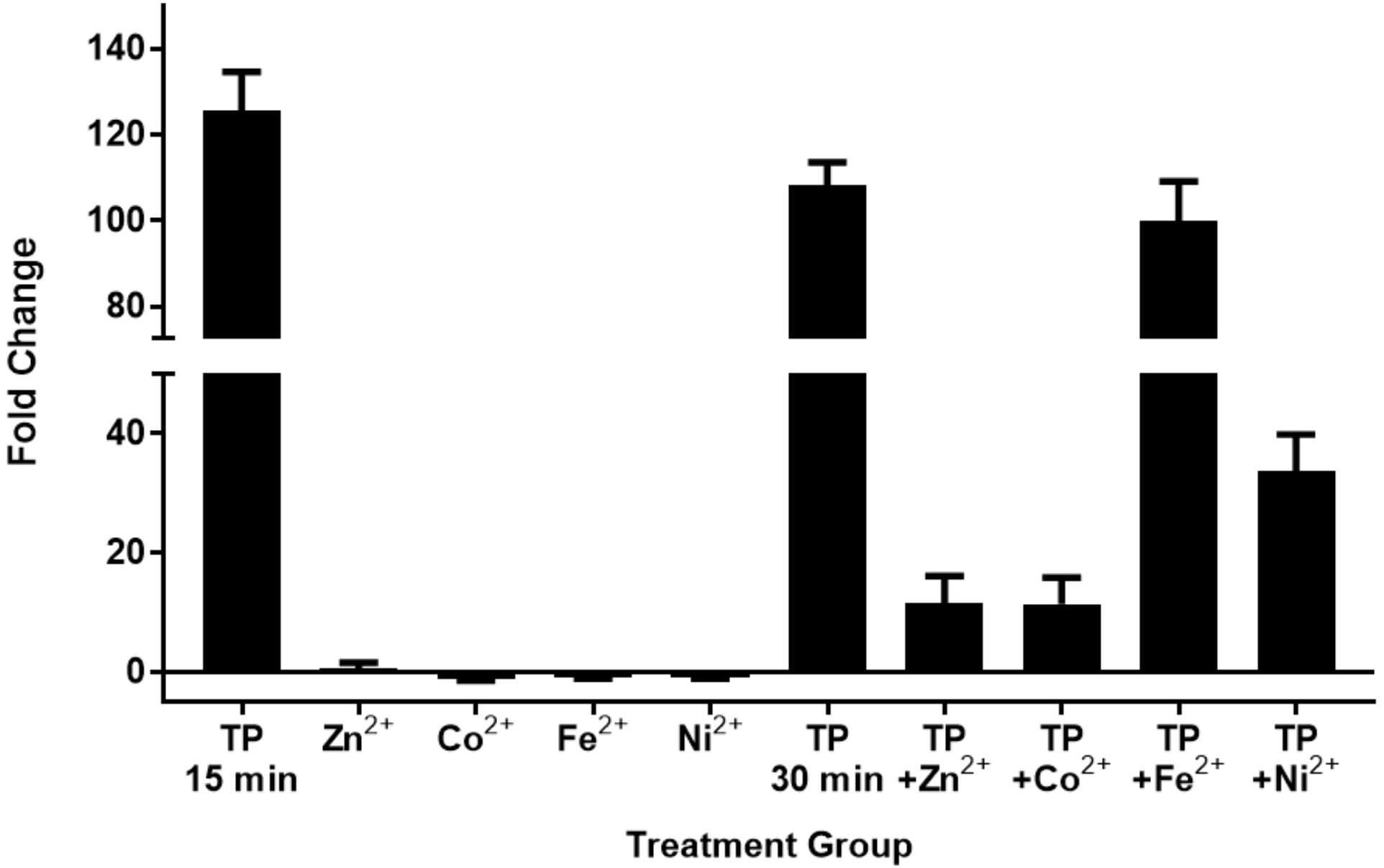
Fold Change
140
120
100
80
40
20
0
TP 15 min
Zn2+
Co2+
Fe2+
Ni2+
TP 30 min
TP +Zn2+
TP +Co2+
TP +Fe2+
TP +Ni2+
Treatment Group

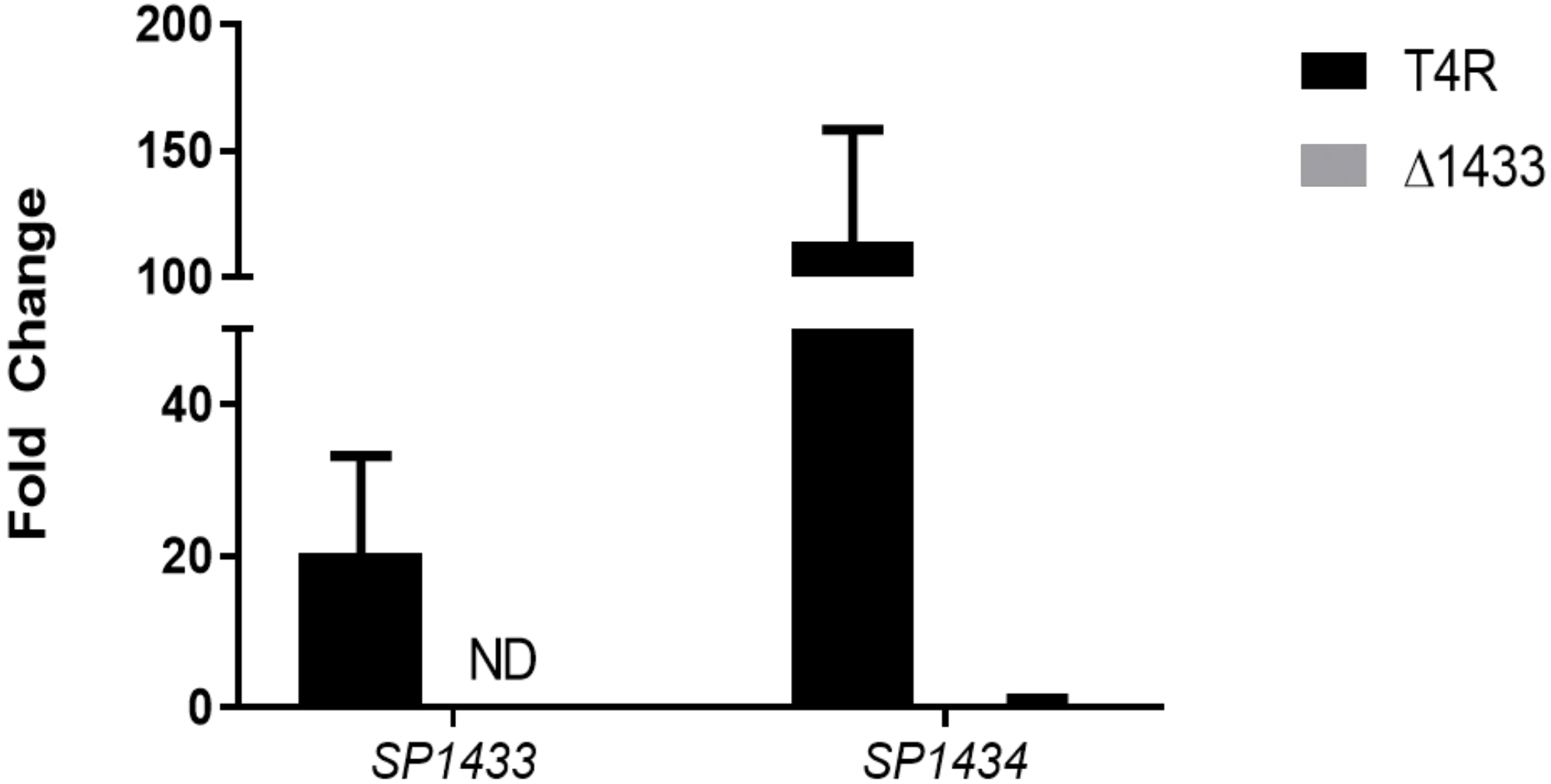
Fold Change
200
150
100
40
20
0
ND
SP1433
SP1434
T4R
Δ1433

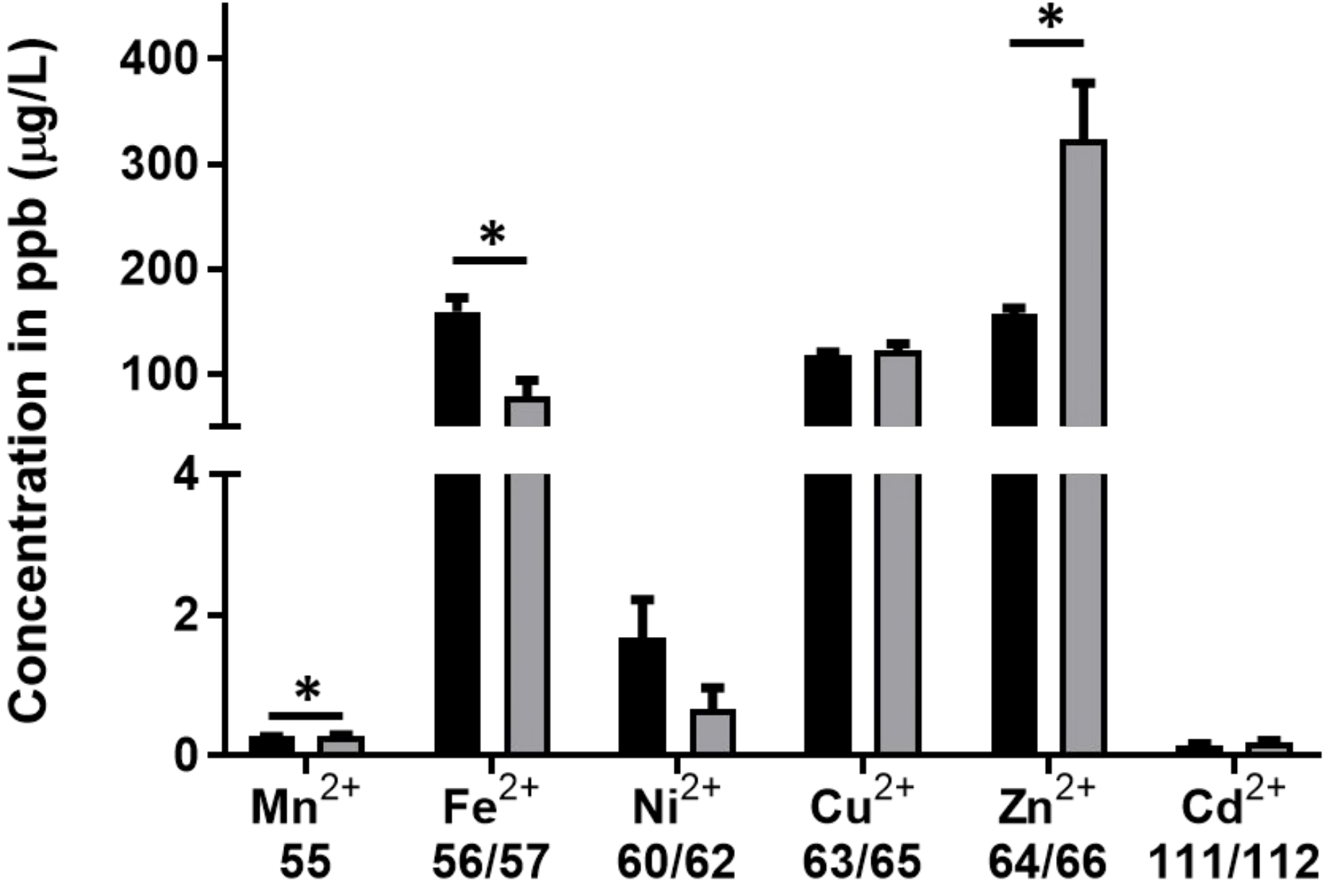
Concentration in ppb (µg/L)
400
300
200
100
4
2
0
*
*
*
Mn2+
55
Fe2+
56/57
Ni2+
60/62
Cu2+
63/65
Zn2+
64/66
Cd2+
111/112

A

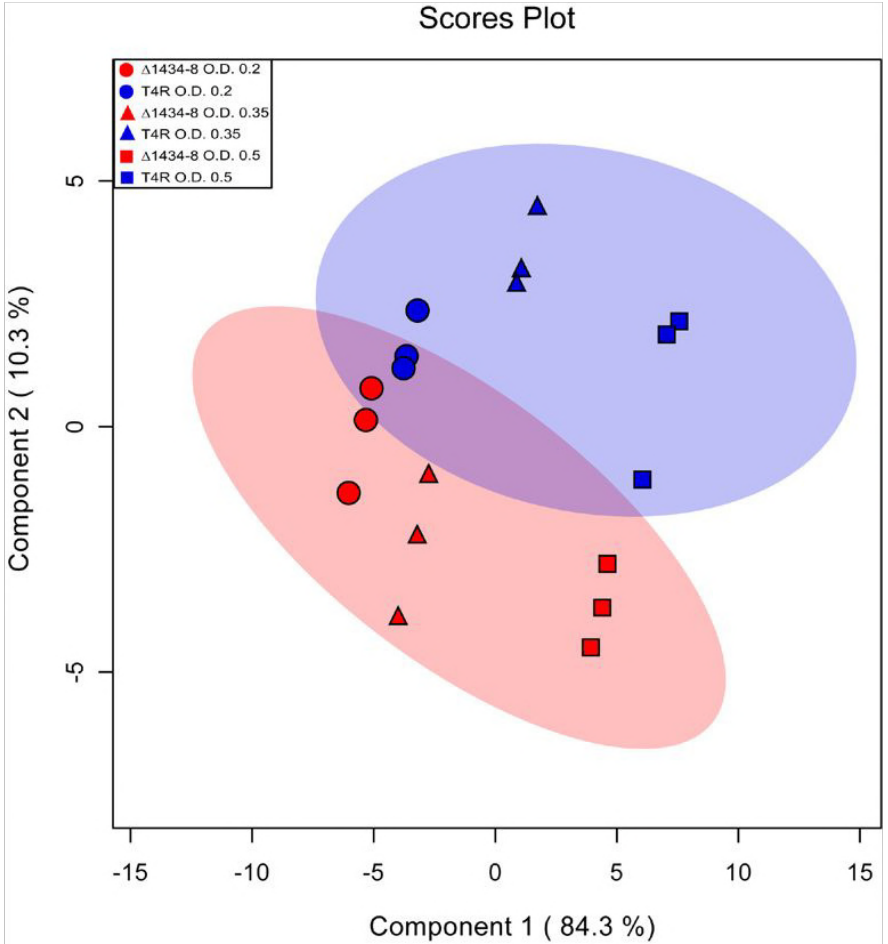
Scores Plot
Δ1434-8 O.D. 0.2
T4R O.D. 0.2
Δ1434-8 O.D. 0.35
T4R O.D. 0.35
Δ1434-8 O.D. 0.5
T4R O.D. 0.5
Component 2 (10.3 %)
Component 1 (84.3 %)
-15
-10
-5
0
5
10
15
5
0
-5

B

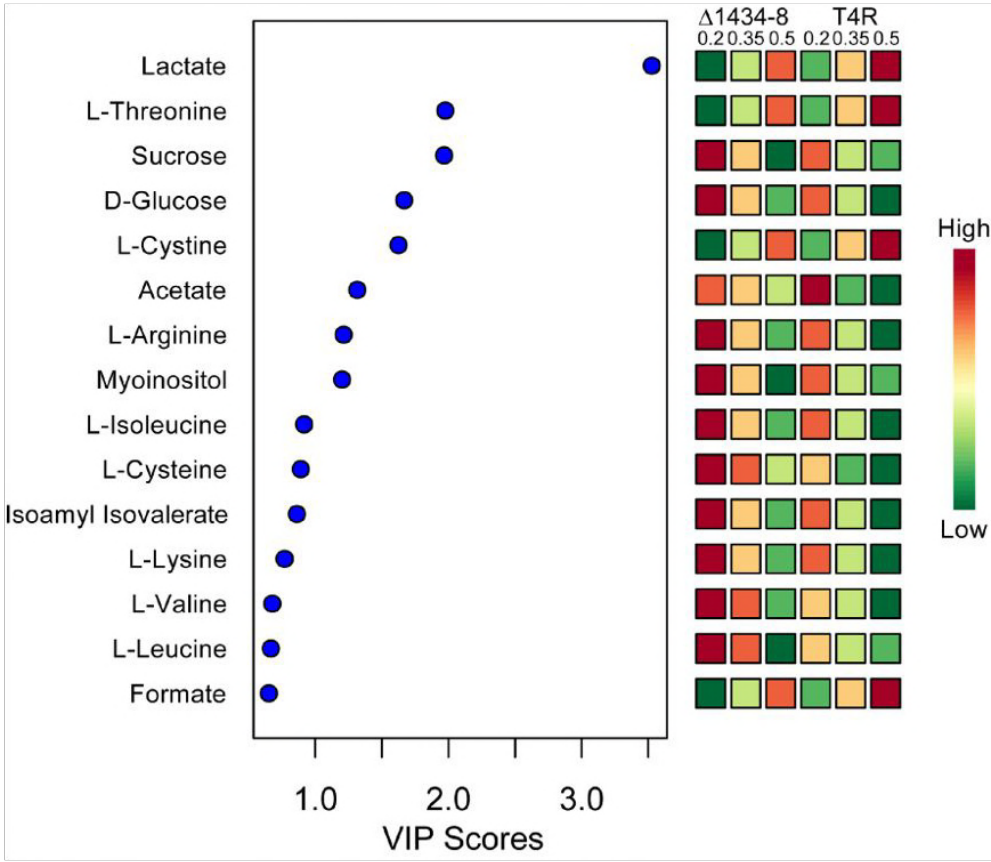
Δ1434-8
T4R
0.2 0.35 0.5 0.2 0.35 0.5
Lactate
L-Threonine
Sucrose
D-Glucose
L-Cystine
Acetate
L-Arginine
Myoinositol
L-Isoleucine
L-Cysteine
Isoamyl Isovalerate
L-Lysine
L-Valine
L-Leucine
Formate
1.0
2.0
3.0
VIP Scores
High
Low

C

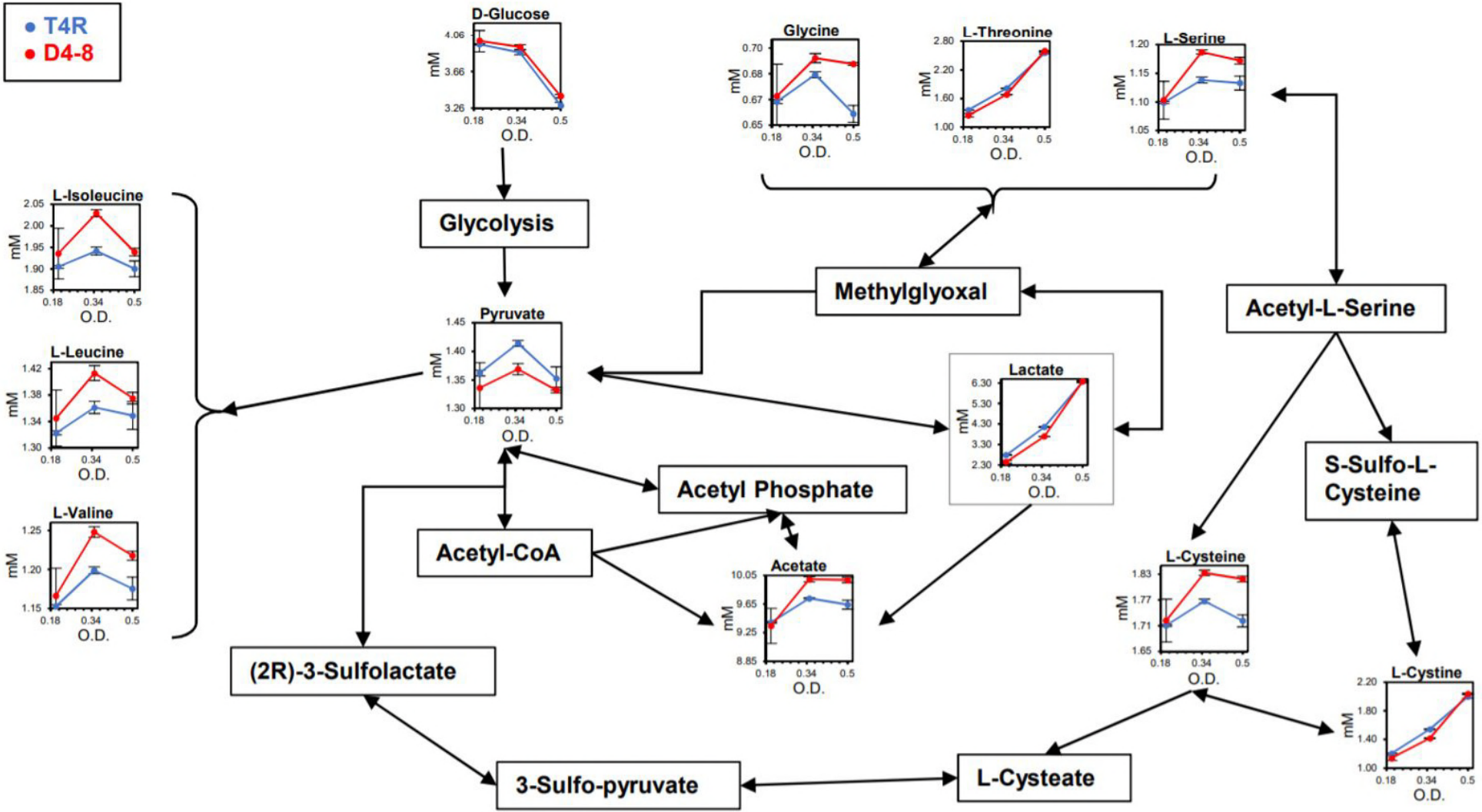
T4R
D4-8
D-Glucose
Glycine
L-Threonine
L-Serine
L-Isoleucine
L-Leucine
L-Valine
Glycolysis
Methylglyoxal
Acetyl-L-Serine
Pyruvate
Lactate
Acetyl Phosphate
S-Sulfo-L-Cysteine
Acetyl-CoA
Acetate
L-Cysteine
(2R)-3-Sulfolactate
L-Cystine
3-Sulfo-pyruvate
L-Cysteate
mM
O.D.

Fold Change	Gene Name	Description
-10.0	SP_1557	uncharacterized protein, DegV (fatty-acid binding protein)
-5.0	AgaB	galactosamine PTS system transporter subunit IIB
-3.3	GatB	Galactose PTS
-2.0	AdhB	alcohol dehydrogenase (zinc)
-2.0	NanU	N-acetylneuraminate ABC transporter substrate-binding protein
-2.0	NanE	N-acetylmannosamine-6-phosphate-2-epimerase
-1.4	RaiA	ribosomal subunit interface protein
-1.3	AdhE	alcohol dehydrogenase (iron)
4.8	RpiA	ribose-5-phosphate isomerase A
-3.3	PiuA	iron ABC-transporter
1.3	GapN	glyceraldehyde-3-phosphate dehydrogenase
-1.7	ArcB	ornithine carbamoyltransferase
5.3	ArtM	ABC-type arginine transport system
-1.4	ClpE	ATP-dependent Clp protease
-11.1	ClpL	ATP-dependent Clp protease ATP-binding subunit
-10.0	PyrK	dihydroorotate dehydrogenase electron transfer subunit, oxidoreductase activity
-10.0	FucD	lactaldehyde dehydrogenase fucose/iron dehydrogenase
-5.0	FolD	tetrahydrafolate dehydrogenase, oxidoreductase activity
-25.0	SP_1690	sugar ABC transporter substrate-binding protein
-14.3	RpmG	50s ribosomal protein L33
-12.5	NanB	neuraminidase B
-12.5	PstS2	phosphate ABC transporter
-10.0	SP_1536	methyltransferase, TrmN6
-10.0	SP_1686	Gfo/Idh/MocA family oxidoreductase
-5.0	AgaS	tagatose-6-phosphate-isomerase
-5.0	SpxA	transcriptional regulator

-5.0	SP_1023	N-acetyltransferase
-5.0	YdhJ	homologous to: HD superfamily phosphodyrolase
-5.0	Gtf1	group 1 glycosyl transferase
-5.0	SP_1943	GNAT family acetyltransferase
-5.0	SP_2073	ABC transporter
-3.3	SP_1114	ABC transporter ATP-binding protein
-3.3	SsuE	NAD(P)H-dependent FMN reducatse
-2.5	SP_0097	integral membrane domain
-2.0	BgaA	beta-galactosidase (galactose metabolism)
-1.7	RplO	50s ribosomal protein L15
-1.4	CbpA	choline binding protein A
-1.3	SP_1804	Alkaline shock protein, YloU
4.8	TehB	tellurite resistance protein (S-adenosylmethionine-dep methyltransferase activity)
5.4	SP_0923	Cof family protein, phosphatase (hydrolase)
7.4	SP_2028	phosphotyrosine protein phosphatase